AIP Journal of Applied Physics

Spectroscopic refractive indices of monoclinic single crystal and ceramic lutetium oxyorthosilicate from 200 to 850nm

Gerald E. Jellison, Eliot D. Specht, Lynn A. Boatner, David J. Singh, and Charles L. Melcher

Citation: J. Appl. Phys. **112**, 063524 (2012); doi: 10.1063/1.4752421
View online: http://dx.doi.org/10.1063/1.4752421
View Table of Contents: http://jap.aip.org/resource/1/JAPIAU/v112/i6
Published by the American Institute of Physics.

Related Articles

Full extraction methods to retrieve effective refractive index and parameters of a bianisotropic metamaterial based on material dispersion models
J. Appl. Phys. 112, 064907 (2012)

GaN-based light emitting diodes with micro- and nano-patterned structures by femtosecond laser nonlinear decomposition
Appl. Phys. Lett. 101, 131103 (2012)

On the method of photoluminescence spectral intensity ratio imaging of silicon bricks: Advances and limitations
J. Appl. Phys. 112, 063116 (2012)

Aluminium doped Zn1−xMgxO—A transparent conducting oxide with tunable optical and electrical properties
Appl. Phys. Lett. 101, 121918 (2012)

Structure and optical band gap of ZnO1−xSx thin films synthesized by chemical spray pyrolysis for application in solar cells
J. Appl. Phys. 112, 063708 (2012)

Additional information on J. Appl. Phys.

Journal Homepage: http://jap.aip.org/
Journal Information: http://jap.aip.org/about/about_the_journal
Top downloads: http://jap.aip.org/features/most_downloaded
Information for Authors: http://jap.aip.org/authors

ADVERTISEMENT

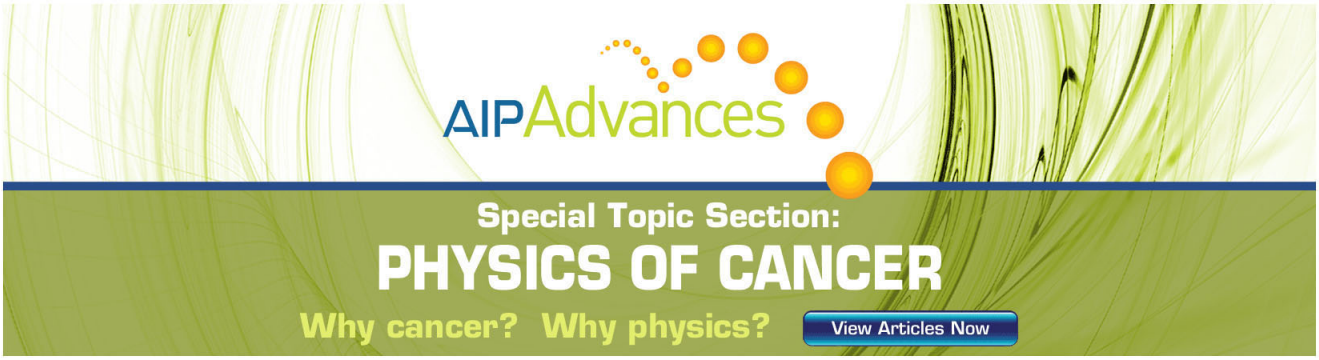

Spectroscopic refractive indices of monoclinic single crystal and ceramic lutetium oxyorthosilicate from 200 to 850 nm

Gerald E. Jellison, Jr.,[1] Eliot D. Specht,[1] Lynn A. Boatner,[1] David J. Singh,[1] and Charles L. Melcher[2]
[1]*Materials Science and Technology Division, Oak Ridge National Laboratory, Oak Ridge, Tennessee 37831, USA*
[2]*Scintillation Materials Research Center, University of Tennessee, Knoxville, Tennessee 37996, USA*

(Received 4 June 2012; accepted 15 August 2012; published online 26 September 2012)

The four real values of the dielectric function tensor of the monoclinic crystal Lu_2SiO_5 or lutetium oxyorthosilicate (LSO) have been determined using generalized ellipsometry from 200 to 850 nm. The three principal values are fit to the Sellmeier model and they indicate that the band gap of LSO is less than ~9 eV. The off-diagonal element ε_{12} is non-zero over the entire spectrum, but it is very close to zero for wavelengths longer than ~400 nm, indicating that structurally monoclinic LSO is nearly optically orthorhombic in this wavelength region. The spectroscopic dielectric functions of three isotropic ceramic LSO samples are presented, which are consistent with the dielectric functions of single-crystal LSO when the effects of optical density are included. As a comparison, the dielectric functions are also determined using relativistic electronic structure and optical calculations based on the recently developed potential functional of Tran and Blaha [Phys. Rev. Lett. **102**, 226401 (2009)].
© *2012 American Institute of Physics*. [http://dx.doi.org/10.1063/1.4752421]

I. INTRODUCTION

Lutetium oxyorthosilicate (LSO, Lu_2SiO_5) doped with cerium is a well-known scintillator used extensively in positron emission tomography (PET) scanners.[1] Crystals of LSO are monoclinic (a = 14.2774 Å, b = 6.6398 Å, c = 10.2464 Å, $\beta = 122.224°$) with space group C2/c and point group C_{2h},[2] corresponding to number 15 in the International Tables for X-Ray Crystallography. The point group has one axis of symmetry with two symmetry operations: a 180° rotation and a mirror plane perpendicular to the symmetry axis.

Although LSO is well known as a scintillator material, much less is known about its optical properties. Since the crystal is monoclinic, there are 4 different dielectric functions ε that are required to describe the material's interaction with light in the wavelength region where the material is transparent.[3–5] That is, the dielectric tensor is given by

$$\varepsilon = \begin{bmatrix} \varepsilon_{11} & \varepsilon_{12} & 0 \\ \varepsilon_{12} & \varepsilon_{22} & 0 \\ 0 & 0 & \varepsilon_{33} \end{bmatrix}, \tag{1}$$

in the principal axis system. Here, we present optical data taken below the fundamental band edge, where LSO is transparent. Above the edge, the values of the dielectric functions are complex, requiring four additional parameters to describe the material.

There is very little work reported in the literature concerning measurements of the dielectric function (or equivalently, the refractive index $n = \varepsilon^{1/2}$) of LSO and none of the results deal with the full spectral complexity of monoclinic LSO. The earliest known values of the refractive index were reported by Anan'eva *et al.*,[6] where they determined 3 different refractive indices at the sodium D line (589.3 nm) using the immersion technique. This work did acknowledge that the optical functions were tensoral, but they did not report the off-diagonal element, nor was the work reported at more than one wavelength. Much later, Mao *et al.*[7] reported a single value of the refractive index at 4 different wavelengths in the visible part of the spectrum (405, 436, 486, and 546 nm) using the V-prism technique, which is similar to the standard minimum deviation technique. While they did perform measurements at more than one wavelength, the single refractive index that was reported ignores the tensoral character of the optical functions of monoclinic LSO.

There have been two reported values of the fundamental band edge of LSO. Optical transmission measurements of a pure LSO crystal resulted in the cutoff of light at ~6.4 eV.[8] The band edge can also be estimated from the Ce excitation spectrum of a Ce-doped LSO crystal, where Kobayashi *et al.*[9] determined a band edge of ~6.2 eV. Indeed, both of these techniques will give a lower bound to the energy of the band edge, but cannot give an exact value, since impurity absorption near the band edge can also contribute to the optical absorption.

Several authors have reported photoluminescence spectra resulting from ultraviolet (UV), vacuum ultraviolet (VUV), and x-ray excitation.[10–13] Kamenskikh *et al.*[10] did state that the band edge of LSO was greater than 6.5 eV, but the other authors did not report a value of the fundamental band edge of LSO. This is not surprising, since photoluminescence can be excited from below-band-gap light.

In this paper, we present spectroscopic generalized ellipsometry measurements of the spectroscopic dielectric function of monoclinic LSO from 200 to 850 nm (6.2 to 1.46 eV). This work is similar to measurements made on other radiation detection materials, including cubic bismuth germanate (BGO),[14] uniaxial bismuth iodide (BiI_3),[15] and monoclinic cadmium tungstate ($CdWO_4$).[5] We show that 4 elements of

 © 2012 American Institute of Physics

the dielectric tensor, as shown in Eq. (1), are required to describe the data, and that the imaginary parts of the dielectric function are zero within error throughout the measured wavelength region. A Sellmeier oscillator and a constant additive term are used to fit the real part of the dielectric function, which indicates that the actual band edge of LSO is $\sim<9$ eV. For comparison purposes, the spectroscopic values of the optical functions of several isotropic ceramic materials made from LSO powder are also included. We also include the results from band structure calculations from which the optical band gap and the spectroscopic dielectric functions can be calculated.

II. EXPERIMENT AND THEORY

A. Samples

A single crystal of LSO was grown using the Czochralski technique in a Cyberstar Oxypuller 05-03 growth station. Commercially obtained lutetium and silicon oxide powders of at least 99.99% purity were mixed and then melted in an iridium crucible. The 60 mm diameter $\times$ 60 mm tall crucible was inductively heated by an 8 kHz power supply. A flowing atmosphere, $\sim$1 l/min, of nitrogen $+\sim$1500 ppm oxygen were continuously monitored with a Dymaxion Dycor residual gas analyzer. The growth was initiated with a LSO seed crystal oriented along the [1 0 0] axis, and a boule of 32 mm diameter was grown at 1.5 mm/h and 10 rpm. Uniform growth was obtained via a control algorithm based on the derivative of the mass of the growing crystal. The sample examined, shown in Fig. 1, was $5 \times 5 \times 12$ mm^3 where the main symmetry axis was nominally along the long edge. Three faces were prepared for spectroscopic ellipsometry measurements using a final Syton polish to minimize the surface roughness. The faces are labeled A, B, and C, where the main crystallographic symmetry axis (b) is nearly perpendicular to the B face, the a-axis is nearly perpendicular to the A face and the reciprocal lattice vector c* is nearly perpendicular to the C-face.

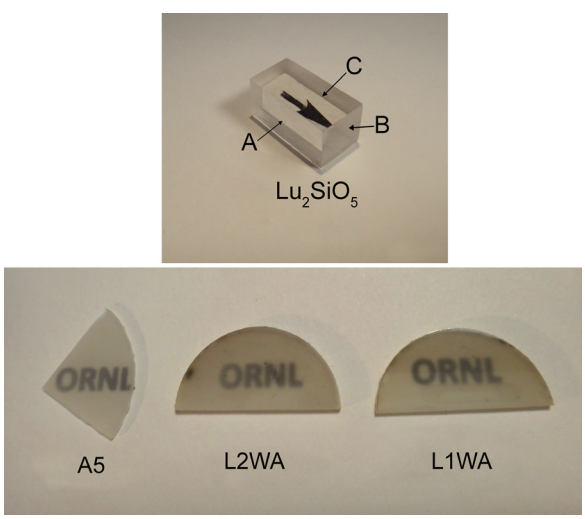

FIG. 1. (Top) Photograph of the single crystal polished sample of LSO, where the three faces examined are labeled A, B, and C. The arrow is drawn on the bottom unpolished face of the crystal and points in the –b direction. (Bottom) Photograph of the three ceramic LSO samples examined in this study, where the treatment characteristics are shown in Table I. All three ceramic LSO samples are transparent in that the lettering can be observed through the crystal with no back lighting.

X-ray diffraction was used to determine the crystallographic axes with respect to each of the polished faces. The sample was mounted on a four-circle diffractometer and tilted using a goniometer head so that the crystal face was normal to the diffractometer ϕ axis: At this orientation, a reflected laser beam is stationary as the ϕ stage is rotated. Crystal orientation is determined using SPEC (Certified Scientific Software). The orientation of a primary reflection [$(\bar{8}02)$ for face A, $(0\bar{2}0)$ for face B, (002) for face C] is found from rocking curves at two azimuths ($\phi = 0$ and $\phi = 90$), and the orientation of a secondary reflection [$(\bar{3}\bar{1}1)$ for faces A and B, (202) for face C] is found from a ϕ scan. At diffractometer settings $\omega = 0$, $\chi = 90$, the crystal face is normal to the scattering vector and SPEC is used to find this crystallographic direction. Angles between facets are calculated from these crystallographic directions using the published LSO crystal structure.[2]

The crystal was nearly perfect to within the resolution of the instrument ($\sim$0.05°) but did have a small region (<20%) on the C-face that was misoriented by 0.3°. The crystal is monoclinic with a unique b-axis. The a- and c-axes are both perpendicular to the b-axis, but the angle between the a- and c-axes is 122.2°. The angles between the faces are determined using the reflection from a laser beam, which can be determined to $\pm$0.1°. The angles between the faces are as follows: A-B: 88.2°, B-C: 92.3°, and C-A: 89.8°. Face A is 3.6° off the [−100] real-space direction, face B is 4.8° off the (0–10)/[0–10] symmetry axis, and the C face is 3.5° off the (001) reciprocal-space plane normal.

Three ceramic cerium-doped LSO:Ce samples were also studied and are shown in Fig. 1. The samples were fabricated using hot pressing of precursor powders as described in Ref. 16. The starting material consisted of a high-quality powder supplied by Nichia Corp. with a particle size $\sim$2 μm and <5% CeO_2. After hot pressing, the resultant material was translucent and x-ray pole figure analysis showed no evidence of texturing.[16] A degree of transparency (as shown in Fig. 1) could be induced via annealing subsequent to the hot pressing step. The formation conditions for the three ceramic samples are summarized in Table I.

B. Generalized ellipsometry

Spectroscopic generalized ellipsometry measurements were made from 200 to 850 nm (6.2 to 1.46 eV) using the two-modulator generalized ellipsometer (2-MGE)[17] on each of the 3 polished faces described above. The procedure is similar to that described in Ref. 5 in that four different 2-MGE measurements were made on each of the three faces, where the sample was rotated 45° for each subsequent measurement for a total of 12 measurements. The initial placement of the crystal was accurate to $\sim$1°, while subsequent placements of the crystal were accurate to $\sim$0.2°. Table II shows the file names, where the letter refers to the face being examined, and the numbers refer to the azimuthal angle of the sample during the measurement. To comply with

TABLE I. LSO transparent polycrystalline ceramic formation conditions.

Sample	L1WA	L2WA	A5
Hot press temperature (°C)	1400	1400	1400
Hot press (kg) 19 mm ID die	800	800	1400
Pressing time (h)	4	4	2
Anneal 1 time (h)	108	216	108
Anneal 1 temperature (°C)	1050	1050	1050
Anneal 1 atm.	Vacuum	Vacuum	Air
Anneal 2 time	32	32	…
Anneal 2 temperature (°C)	1050	1050	…
Anneal 2 atm.	H_2O vapor	H_2O vapor	…
Anneal 3 time (h)	32	32	…
Anneal 3 temperature (°C)	1050	1050	…
Anneal 3 atm.	Air	Air	…

standard notation for dielectric tensors, a permutation operator is applied to transform the axis system from (a, b, c*) to (1, 2, 3), where the unique axes are b in the crystallographic system and 3 in the dielectric tensor system. The table also includes the Euler angles of the crystallographic axis system with respect to the laboratory coordinate system, where the Euler angles are defined in Ref. 18.

Figure 2 shows examples of the data obtained for two different orientations of the LSO crystal. Although the raw data are determined in the NSC format (see Ref. 17), it is often convenient to convert the data to the ρ representation when there is no depolarization present. In this representation, the regular ellipsometric parameters are expressed as

$$\rho = \frac{r_{pp}}{r_{ss}} = \tan(\psi_{el})\exp(i\Delta_{el}) = \frac{C + iS}{1 + N}, \qquad (2)$$

where r_{pp} (r_{ss}) is the complex reflection coefficient for light polarized parallel (perpendicular) to the plane of incidence. The standard ellipsometric angles are given by ψ_{el} and Δ_{el}, $N = \cos(2\psi_{el})$, $S = \sin(2\psi_{el})\sin(\Delta_{el})$, and $C = \sin(2\psi_{el})\cos(\Delta_{el})$. If the sample is anisotropic, then it is possible for pure p-(s-) polarized light to result in some s-(p-) polarized light upon reflection (cross polarization). The cross polarization reflection ratios are given by $\rho_{ps} = r_{ps}/r_{ss}$ and $\rho_{ps} = r_{sp}/r_{ss}$. As can be seen, the ellipsometric data are featureless apart from dispersion. In addition, the imaginary parts of ρ_{sp} and ρ_{ps} are all 0 within error, so they are not shown. No band structure features are observed in the wavelength region examined.

TABLE II. The 12 different configurations measured, including the surface roughness, the Euler angles θ, ϕ, and ψ, and the resulting χ^2 of the fit. The average roughness thickness errors are from the fitting procedure described in the text, while the average angular error results from the initial placement of the crystal on the sample stage. The average of the individual χ^2 is 1.08.

File name	Roughness (nm)	θ	ϕ	ψ	χ^2
B000	3.73	175.1	95.8	−176.4	1.65
B045	3.63	175.1	50.8	−176.4	0.76
B090	3.60	175.1	5.8	−176.4	0.64
B135	3.70	175.1	−39.2	−176.4	1.90
C000	2.55	87.2	87.0	−91.9	0.79
C045	2.47	90.2	85.9	−47.0	1.12
C090	2.44	93.0	87.2	−2.0	0.91
C135	2.39	94.1	90.2	43.0	0.76
A000	3.31	87.2	−3.0	−91.9	0.71
A045	3.10	90.2	−4.1	−47.0	1.95
A090	2.82	93.0	−2.8	−2.0	0.84
A135	2.77	94.1	0.2	43.0	0.94
Average error	0.02	1.0	1.0	1.0	—

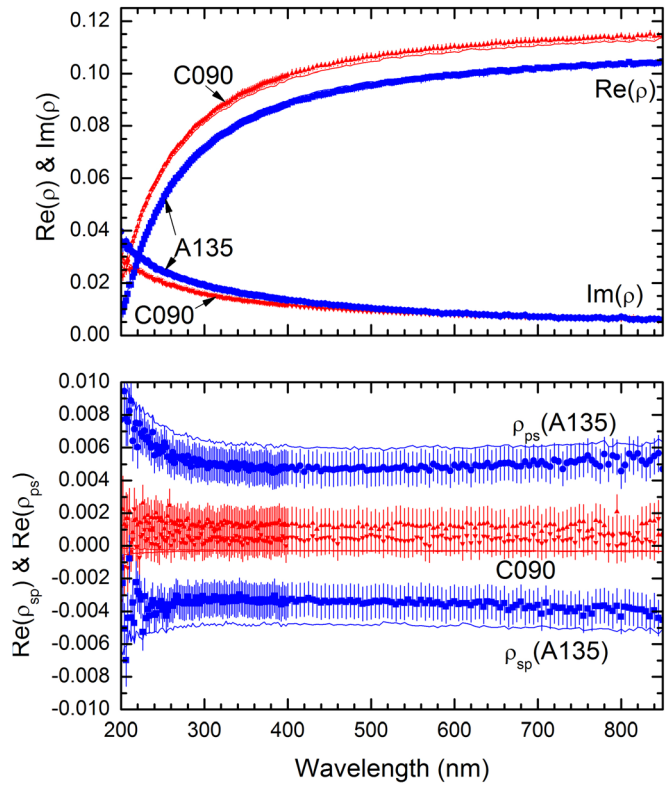

FIG. 2. The values of the ellipsometric parameters in the ρ representation for the crystalline LSO sample aligned at 135° on the A face (A135) and at 90° on the C face (C090). The error bars show both systematic and stochastic errors, discussed in the text. The values of the reduced χ^2 were 0.94 (A135) and 0.91(C090), indicating a good fit to the data.

The error limits of the data are $\sim\pm0.001$ in the ρ representation, as shown in Fig. 2. For wavelengths longer than $\sim$240 nm, the random component of the error is relatively small ($\sim$0.0003), while the estimated systematic component ($\sim$0.001) dominates. The systematic component of the error stems from misorientation of the crystal on the sample stage, errors in the angle of incidence, polarizer and photoelastic modulator (PEM) alignment, and small drifts in the 2-MGE system.

Since each 2-MGE measurement determines 6 parameters at each wavelength (real and imaginary parts of ρ, ρ_{ps}, and ρ_{sp}), the 12 spectra from different orientations of the crystal yield a total of 72 measurements at each wavelength. As described in Ref. 5, the spectroscopic values of the 4 real and 4 imaginary parts of the dielectric function tensor are determined from the 2-MGE data by a linear least-square fitting procedure, where the error limits of the data are included in the fit. Since 8 parameters are determined from 72 data points, the system is over-determined. Surface roughness in incorporated into the fitting procedure by modeling the near-surface region with a simple 3-medium model: air/surface roughness/LSO. The surface roughness is modeled using the

Bruggeman effective medium approximation[19] with 50% voids and 50% LSO, where the dielectric functions of LSO in the surface roughness region are the spectroscopic average of the three principal values ε_{11}, ε_{22}, and ε_{33}. Separate fits of each data set were performed to determine the surface roughness thickness, shown in Table I, where the optical functions of the LSO material for that orientation of the crystal are modeled using the Sellmeier approximation

$$\varepsilon = n^2 = D + \frac{A\lambda^2}{\lambda^2 - \lambda_o^2}. \quad (3)$$

The optical functions of the three isotropic ceramic scintillators were also determined using the 2-MGE. As expected, no cross-polarization was observed, indicating that the samples were macroscopically isotropic. The values of the optical functions are determined from the ellipsometry data by modeling the system as air/surface roughness/ceramic LSO, where the surface roughness is modeled as described above and the ceramic LSO is modeled using the Sellmeier approximation (Eq. (3)).

C. Band structure calculations

The optical properties are calculated from first principles. Optical properties depend on a correct description of the band structure, and, in particular, on the band gaps of materials. Here, we employed a recently developed potential functional, denoted "TB-mBJ."[20] This functional, which is a modified Becke-Johnson type potential gives band gaps and related properties in close agreement with experiment for insulators and semiconductors.[20–23] Optical properties for a number of halide scintillators obtained with this functional are in close agreement with experiment.[24,25] The approach used is similar to that of Ref. 5. Specifically, we used the linearized augmented planewave (LAPW) method, as implemented in the WIEN2k code.[26] The calculations are performed using the experimental lattice parameters of LSO, where the internal atomic coordinates were obtained by total energy minimization with the standard generalized gradient approximation (PBE functional). These atomic coordinates are in good agreement with experimental values of Gustafsson *et al.*[2] (see Table III). We then used this structure for the optical calculation with the TB-mBJ potential functional and included spin-orbit interactions. The optical calculation was performed using electric dipole matrix elements between valence and conduction band states as implemented in the optical package of WIEN2k.

III. RESULTS AND DISCUSSION

A. Spectroscopic ellipsometry

Figure 3 shows the principal values of the dielectric function of single-crystal LSO (c-LSO) from 200 to 850 nm, as well as the dielectric functions of the three ceramic samples examined. The imaginary part was determined to be zero within error over the entire examined spectral region and it is not shown. The values of ε_{33} (along the symmetry axis) are less than the values for the other two principal values of the dielectric function, but the values of ε_{22} (along the a-axis) are nearly equal to the values of ε_{33}. The values of ε_{11} (along the reciprocal lattice vector c*) are somewhat larger than the other two values. The off-diagonal term of the dielectric tensor ε_{12} for c-LSO is shown in Fig. 4 and is clearly non-zero near 200 nm but quickly goes to $\sim -0.011 \pm 0.005$ as the wavelength is increased. The fact that ε_{12} is nearly constant over a wide wavelength range means that a rotation of the coordinate system of $\sim -10°$ renders the dielectric tensor diagonal, and therefore optically orthorhombic, over this wavelength range. At shorter wavelengths, the required rotation is more negative, going to $-22°$ at 200 nm. The principal values of the dielectric function can be converted to refractive indices taking the square root: $n_{ii} = \sqrt{\varepsilon_{ii}}$, where i = 1, 2, 3 and are shown for c-LSO in Fig. 5.

The values of the dielectric functions of the ceramic materials are also shown in Fig. 3. Since these materials are isotropic, there is only a single value of the dielectric function. If the ceramic material were perfectly compressed with randomly oriented crystallites and no voids, one would

TABLE III. Internal coordinates in LSO as obtained from first principles structure energy minimization at 0 K (DFT) in comparison with the ambient temperature experimental structure from diffraction [2]. Here, we use setting C12/c of space group 15.

	DFT			Experiment [2]		
	X	Y	Z	X	Y	Z
Lu1	0.5369	0.7568	0.4667	0.5373	0.7559	0.4671
Lu2	0.1403	0.3769	0.8363	0.1409	0.3774	0.8364
Si	0.3177	0.5915	0.1930	0.3179	0.5917	0.1931
O1	0.4117	0.5060	0.3633	0.4112	0.5062	0.3620
O2	0.3803	0.7897	0.1758	0.3802	0.7883	0.1762
O3	0.2015	0.6498	0.1766	0.2023	0.6490	0.1768
O4	0.2985	0.4281	0.0618	0.2984	0.4289	0.0630
O5	0.0180	0.4030	0.8980	0.0177	0.4034	0.8975

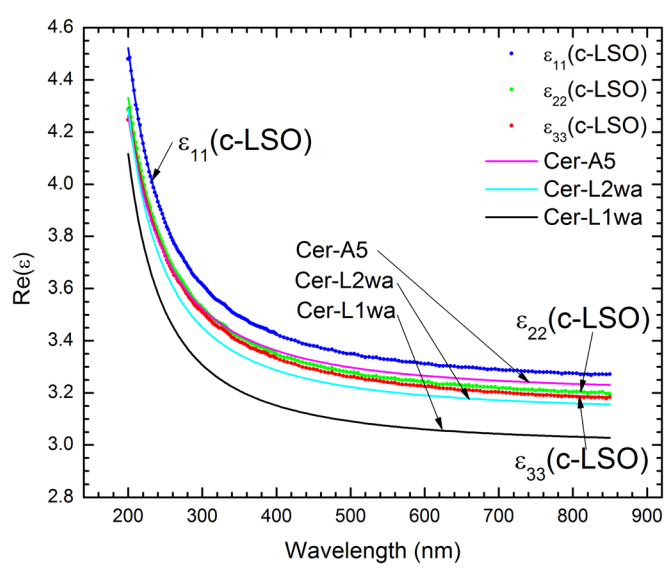

FIG. 3. The dielectric function of LSO as a function of wavelength. The three principal values of the dielectric tensor for crystalline are shown with data points and labeled with (c-LSO), while the values for three different LSO ceramic materials are shown with solid lines and labeled with "Cer-."

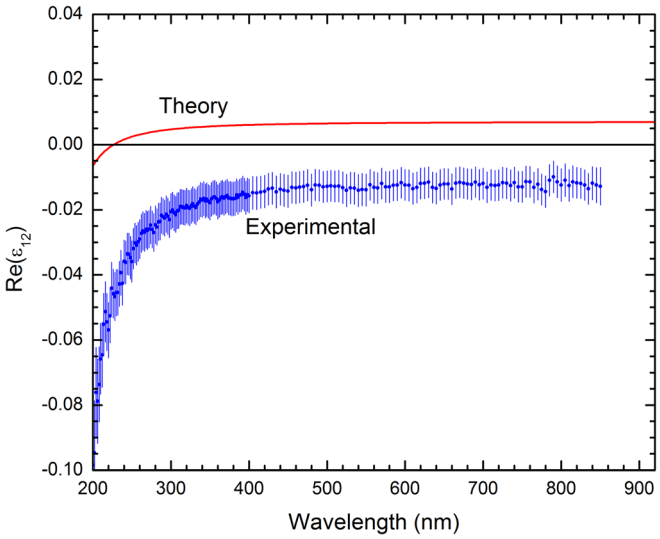

FIG. 4. The off-diagonal tensor element of the dielectric tensor for crystalline LSO.

expect the dielectric function to be the average of the three principal components in the rotated reference frame. As can be seen from Fig. 3, the values of the dielectric function for the ceramic material A5 are very close to this value, while L2wa is only slightly less than the average of ε_{11}, ε_{22}, and ε_{33} of c-LSO. On the other hand, the dielectric function of ceramic L1wa is considerably less than the average dielectric function of c-LSO. The differences in the spectroscopic refractive indices of the three ceramic materials can be understood from the formation conditions shown in Table I. Sample A5 was hot pressed at the highest pressure and, therefore, would be the densest, resulting in the highest refractive index. Sample L1wa was annealed only half as long as sample L2wa, which could also result in a lower optical density and consequently a lower refractive index, as observed.

Given that c-LSO is monoclinic, it is somewhat surprising that the ceramic material made from powder exhibits the degree of transparency evident in Fig. 1. In many ceramic materials made from low-symmetry crystals, the interface regions from different crystallites will be very complicated optically, since the optical behavior will depend upon the different dielectric functions and crystallographic orientations of the crystallites. The similarity of the three principal values of the dielectric tensor of c-LSO, and the fact that the material is nearly optically orthorhombic in the visible part of the spectrum may facilitate the formation of a nearly transparent ceramic from c-LSO powder.

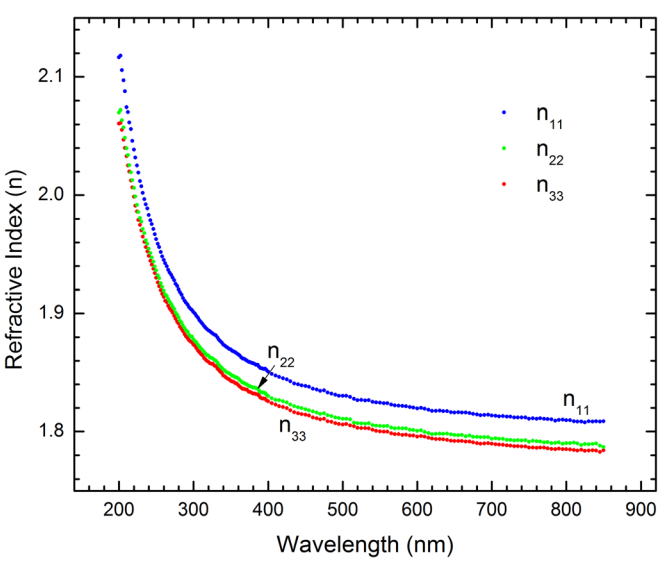

FIG. 5. The three principal values of the refractive index of LSO.

The results of c-LSO presented here can be compared with the existing values of the refractive index of LSO found in the literature. As noted above, the oldest values were measured by Anan'eva *et al.*[6] using the immersion technique. These measurements were performed at the sodium D line (589 nm), where they found 3 values of the refractive index: 1.825, 1.803, and 1.797. The three values found from this work at 589 nm are $n_{11} = 1.821$, $n_{22} = 1.803$, and $n_{33} = 1.797$ with an error of 0.002. Therefore, these results compare well with those of Anan'eva *et al.*

More recently, Mao *et al.*[7] measured the refractive index of LSO at several wavelengths using the V-prism technique, where they obtained a single value at each wavelength. Reference 7 makes no mention of the orientation of the crystal or the polarization state of the probe light, so separate determinations of n_{11}, n_{22}, and n_{33} are not possible. These data are compared with the results from this work in Table IV. Mao's values compare well with the n_{22} values from this work.

The principal values of the dielectric function of c-LSO and the single value of the dielectric function of the ceramic materials can be fit to the Sellmeier model shown in Eq. (3), where the fitted values are shown in Table V. The parameter λ_o is the resonant wavelength of the Sellmeier approximation and therefore a measure of the upper limit of the energy of the direct band gap of LSO. As can be seen, the values of λ_o lie in the range 129.3 to 144.2 nm (9.6 to 8.6 eV). These values are considerably higher than the previously reported energies (6.4 and 6.2 eV from Refs. 8 and 9, respectively) and indicate that the actual band gap of LSO may be somewhat greater than previously thought.

B. Band structure calculations

The density of states is calculated using the TB-mBJ potential and is shown in Fig. 6 along with results for the PBE generalized gradient approximation. Note that the conduction band position is quite different for the TB-mBJ and

TABLE IV. The principal values of the refractive indices of LSO at selected wavelengths. The average values of the three principal values of the refractive index are shown in the column ⟨n⟩. For comparison, the values as measured by Mao *et al.*[7] are shown in the last column.

Wavelength (nm)	n_{11}	n_{22}	n_{33}	⟨n⟩	Mao *et al.*[7]
405	1.849	1.828	1.824	1.834	1.833
436	1.841	1.822	1.816	1.826	1.822
486	1.832	1.813	1.808	1.818	1.813
546	1.825	1.805	1.801	1.810	1.806

TABLE V. Fitted parameters of the values of the Sellmeier model for the principal values of the dielectric function of LSO as determined from the experiment and from the theoretical calculations. The values of the Sellmeier fits are also included for the 3 ceramic samples of LSO.

	A	λ_o	D
c-LSO ε_{11}	1.44 ± 0.01	137.6 ± 0.3	1.80 ± 0.01
c-LSO ε_{22}	1.54 ± 0.02	131.4 ± 0.4	1.63 ± 0.02
c-LSO ε_{33}	1.60 ± 0.02	129.3 ± 0.5	1.55 ± 0.02
c-LSO ε_{11} theory	1.101	127.2	1.667
c-LSO ε_{22} theory	1.136	122.2	1.592
c-LSO ε_{33} theory	1.111	122.7	1.600
Ceramic A5	1.31 ± 0.13	134.1 ± 4.3	1.89 ± 0.13
Ceramic L1wa	1.03 ± 0.13	144.2 ± 5.4	1.96 ± 0.14
Ceramic L2wa	1.13 ± 0.09	142.6 ± 3.3	2.00 ± 0.09

the PBE calculations. This reflects the common limitation of the PBE approach in that it often underestimates the band gap of semiconductors and insulators. Using the actual calculated bands, the fundamental band gap of LSO is calculated to be 6.7 eV and it is direct at the Γ-point. The calculated principal values of the dielectric functions are shown in Fig. 7, along with the experimental values previously presented in Fig. 3. The calculated values of the off-diagonal ε_{12} are shown in Fig. 4 along with the experimental values.

As can be seen from Fig. 7 and the fitted parameters from the Sellmeier fit presented in Table V, the magnitudes of the principal values of the calculated dielectric function tensor are significantly less than the experimental values. This difference is due to a characteristic of the first principles calculations, where the degree of covalency of the bonds is moderately overestimated. However, the order of the calculated principal values of the dielectric function do agree with the experimentally determined values ($\varepsilon_{11} > \varepsilon_{22} > \varepsilon_{33}$). Moreover, both theory and experiment show that the three principal values of the dielectric function are nearly equal, and that ε_{12} is small. This behavior is similar to the results determined from calculations of many halides but quite different from oxides, such as monoclinic $CdWO_4$. The small differences between the principal values of the dielectric functions and the small value of the off-diagonal ε_{12} from both theory and

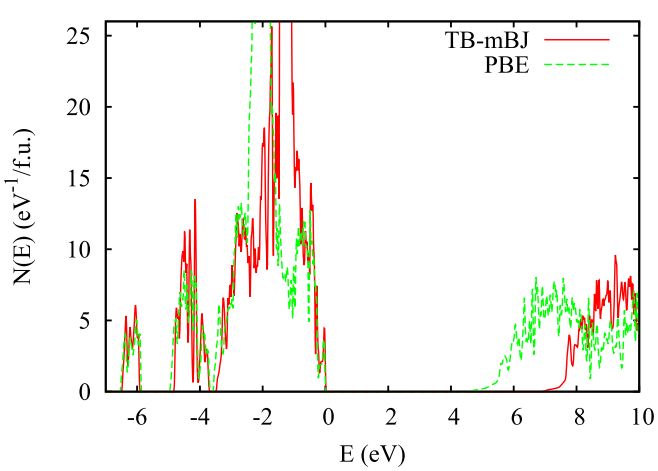

FIG. 6. Density of states of LSO determined from band structure calculations. Note the larger improved band gap with the TB-mBJ potential.

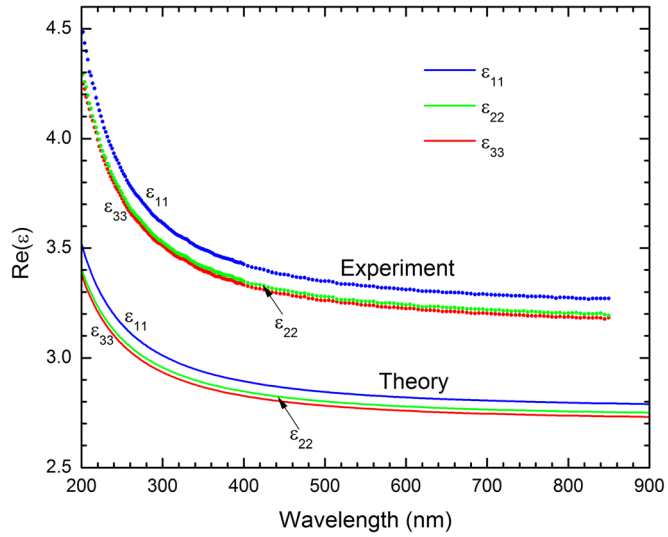

FIG. 7. Dielectric function of LSO calculated using band structure calculations compared with the experimental values (also shown in Fig. 3).

experiment point to the possibility of making high-quality LSO ceramic scintillators, which has been experimentally verified.

IV. CONCLUSIONS

The optical functions of LSO have been determined using spectroscopic generalized ellipsometry from 200 to 850 nm (6.2 to 1.46 eV). The analysis of the data shows that there are 4 real values of the dielectric function in this wavelength range, as required for monoclinic crystals. The spectroscopic principal values of the dielectric function are unequal and are ordered $\varepsilon_{11} > \varepsilon_{22} > \varepsilon_{33}$, where ε_{22} and ε_{33} are nearly equal, and ε_{11} is somewhat larger than ε_{22} and ε_{33}. The off-diagonal element ε_{12} is non-zero but is very small. The principal values of the dielectric function can be fit to a Sellmeier approximation and indicate that the resonant wavelength $\lambda_o \sim 9.1$ eV, which gives an upper limit to the band edge.

From both experiment and theory, the principal values of the dielectric function of LSO are very similar one to another, and the off-diagonal element ε_{12} is close to zero. This behavior explains the observation that high quality translucent ceramic scintillators can be made from LSO powder. Generalized ellipsometry measurements were also made on a series of ceramic LSO materials. The optical functions of the ceramic materials were isotropic and similar to the crystalline values but varied depending on fabrication conditions. Materials that were treated in such a way would reasonably result in higher density material had higher values of the dielectric function, as would be expected.

Previous measures of the band edge of LSO indicated that the value is greater than the previous values of 6.2-6.4 eV. The values of the Sellmeier resonant wavelength λ_o, which gives an upper limit to the band edge, are in the range of 129.3 to 144.2 nm (9.6-8.6 eV) for the crystalline principal values and the values determined from the ceramic LSO material. The theoretical value discussed in this paper gives a value of 6.7 eV, which lies between the two sets of experimental

values. Consequently, additional measurements are needed to give a more accurate value of the band edge of LSO.

ACKNOWLEDGMENTS

This work was supported by the Department of Energy, NNSA, Office of Non-Proliferation Research and Development, NA-22.

This manuscript has been authored by UT-Battelle, LLC, under Contract No. DE-AC05-00OR22725 with the U.S. Department of Energy. The United States Government retains and the publisher, by accepting the article for publication, acknowledges that the United States Government retains a non-exclusive, paid-up, irrevocable, world-wide license to publish or reproduce the published form of this manuscript, or allow others to do so, for United States Government purposes.

[1]C. L. Melcher and J. S. Schweitzer, "Cerium-doped lutetium oxyorthosilicate: A fast, efficient new scintillator," IEEE Trans. Nucl. Sci. **39**, 502–505 (1992).
[2]T. Gustafsson, M. Klintenberg, S. E. Derenzo, M. J. Weber, and J. O. Thomas, "Lu_2SiO_5 by single-crystal X-ray and neutron diffraction," Acta Cryst. C **57**, 668–669 (2001).
[3]G. N. Ramachandran and S. Ramaseshan, "Crystal optics," in *Handbuch der Physik*, edited by S. Fluegge (Springer, Berlin, 1961), Vol. 25/1, p. 1.
[4]R. W. Collins and A. S. Ferlauto, *in Handbook of Ellipsometry*, edited by H. G. Tompkins and E. A. Irene (William Andrew, Norwich, NY, 2005), Chap. 2.
[5]G. E. Jellison, Jr., M. A. McGuire, L. A. Boatner, J. D. Budai, E. D. Specht, and D. J. Singh, "Spectroscopic dielectric tensor of monoclinic crystals: $CdWO_4$," Phys. Rev. B **84**, 195439 (2011).
[6]G. V. Anan'eva, A. M. Korovkin, T. I. Merkulyaeva, A. M. Morozova, M. V. Petrov, I. R. Savinova, V. R. Startsev, and P. P. Feofilov, "Growth of lanthanide oxyorthosilicate single crystals, and their structural and optical characteristics," Izv. Akad. Nauk SSSR, Neoganischeskie Mater. **17**, 1037 (1981).
[7]R. Mao, L. Zhang, and R.-Y. Zhu, "Optical and scintillation properties of inorganic scintillators in high energy physics," IEEE Trans. Nucl. Sci. **55**, 2425–2431 (2008).
[8]A. Lempicki and J. Glodo, "Ce-doped scintillators: LSO and LuAP," Nucl. Instrum. Meth. Phys. Res. A **416**, 333–344 (1998).
[9]M. Kobayashi, M. Ishii, and C. L. Melcher, "Radiation damage of a cerium-doped lutetium oxyorthosilicate single crystal," Nucl. Instrum. Methods Phys. Res. A **333**, 509–512 (1993).
[10]I. A. Kamenskikh, V. V. Mikhailin, I. H. Munro, D. Y. Petrovykh, D. A. Shaw, P. A. Studenikin, A. N. Vasil'ev, I. A. Zagumennyi, and Yu. D. Zavartsev, Radiat. Eff. Defects Solids **135**, 391–396 (1995).
[11]W. Drozdowski, A. J. Wojtowicz, D. Disniewski, P. Szupryczynski, S. Janus, J.-L. Lefaucheur, and Z. Gou, J. Alloys Compd. **380**, 146–150 (2004).
[12]C. Shi, B. Liu, G. Zhang, Z. Qi, G. Ren, Y. Tao, and J. Xu, J. Electron Spectrosc. Relat. Phenom. **144–147**, 905–908 (2005).
[13]B. Liu, C. Shi, M. Yin, Y. Fu, G. Zhang, and G. Ren, J. Lumin. **117**, 129–134 (2006).
[14]G. E. Jellison, Jr., S. Auluck, D. J. Singh, and L. A. Boatner, "Optical properties of bismuth germanate," J. Appl. Phys. **107**, 013514 (2010).
[15]G. E. Jellison, Jr., J. O. Ramey, and L. A. Boatner, "Optical functions of BiI_3 as measured by generalized ellipsometry," Phys. Rev. B **59**, 9718–9721 (1999).
[16]D. J. Wisniewski, L. A. Boatner, J. S. Neal, G. E. Jellison, J. O. Ramey, A. North, M. Wisniewska, A. E. Payzant, J. Y. Howe, A. Lempicki, C. Brecher, and J. Glodo, "Development of novel polycrystalline ceramic scintillators," IEEE Trans. Nucl. Sci. **55**, 1501–1508 (2008).
[17]G. E. Jellison, Jr. and F. A. Modine, "Two-modulator generalized ellipsometry: Experiment and calibration," Appl. Opt. **36**, 8184–8189 (1997); "Two-modulator generalized ellipsometry: Theory," Appl. Opt. **36**, 8190–8198 (1997).
[18]H. Goldstein, *Classical Mechanics* (Addison-Wesley, Cambridge, 1950).
[19]D. A. G. Bruggeman, Ann. Phys. (Berlin) **24**, 636 (1935).
[20]F. Tran and P. Blaha, Phys. Rev. Lett. **102**, 226401 (2009).
[21]D. J. Singh, Phys. Rev. B **82**, 205102 (2010).
[22]D. Koller, F. Tran, and P. Blaha, Phys. Rev. B **83**, 195134 (2011).
[23]Y. S. Kim, M. Marsman, G. Kresse, F. Tran, and P. Blaha, Phys. Rev. B **82**, 205212 (2010).
[24]D. J. Singh, Phys. Rev. B **82**, 155145 (2010).
[25]G. E. Jellison, Jr., L. A. Boatner, J. O. Ramey, J. A. Kolopus, L. A. Ramey, and D. J. Singh, J. Appl. Phys. **111**, 043521 (2012).
[26]P. Blaha, K. Schwarz, G. Madsen, D. Kvasnicka, and J. Luitz, *WIEN2k: An Augmented Planewave + Local Orbitals Program for Calculating Crystal Properties* (Technische Universitat Wien, Vienna, Austria, 2001).